The kilohertz quasi-periodic oscillations during the Z and atoll phases of the unique transient XTE J1701-462

Sanna, Andrea; Mendez, Mariano; Altamirano, Diego; Homan, Jeroen; Casella, Piergiorgio; Belloni, Tomaso; Lin, Dacheng; van der Klis, Michiel; Wijnands, Rudy

Published in:
Monthly Notices of the Royal Astronomical Society

DOI:
10.1111/j.1365-2966.2010.17145.x

Monthly Notices
of the
ROYAL ASTRONOMICAL SOCIETY

Mon. Not. R. Astron. Soc. **408,** 622–630 (2010) doi:10.1111/j.1365-2966.2010.17145.x

The kilohertz quasi-periodic oscillations during the Z and atoll phases of the unique transient XTE J1701−462

Andrea Sanna,[1⋆] Mariano Méndez,[1] Diego Altamirano,[2] Jeroen Homan,[3] Piergiorgio Casella,[4] Tomaso Belloni,[5] Dacheng Lin,[6] Michiel van der Klis[2] and Rudy Wijnands[2]

[1]*Kapteyn Astronomical Institute, University of Groningen, PO BOX 800, 9700 AV Groningen, the Netherlands*
[2]*Sterrenkundig Instituut Anton Pannekoek, Science Park 904, 1098 XH Amsterdam, the Netherlands*
[3]*MIT Kavli Institute for Astrophysics and Space Research, 70 Vassar Street, Cambridge, MA 02139, USA*
[4]*School of Physics and Astronomy, University of Southampton, Southampton, Hampshire SO17 1BJ*
[5]*INAF-Osservatorio Astronomico di Brera, Via E. Bianchi 46, I-23807 Merate (LC), Italy*
[6]*Centre d'Etude Spatiale des Rayonnements, UMR 5187, 9 av. du Colonel Roche, BP 44346, 31028 Toulouse Cedex 4, France*

Accepted 2010 June 4. Received 2010 May 18; in original form 2010 March 15

ABSTRACT

We analysed 866 observations of the neutron star low-mass X-ray binary XTE J1701−462 during its 2006–2007 outburst. XTE J1701−462 is the only example so far of a source that during an outburst showed, beyond any doubt, spectral and timing characteristics both of the Z and atoll type. There are 707 *RXTE* observations (∼2.5 Ms) of the source in the Z phase and 159 in the atoll phase (∼0.5 Ms). We found, respectively, pairs of kilohertz quasi-periodic oscillations (kHz QPOs) in eight observations during the Z phase and single kHz QPO in six observations during the atoll phase. Using the shift-and-add technique, we identified the QPO in the atoll phase as the lower kHz QPO. We found that the lower kHz QPO in the atoll phase has a significantly higher coherence and fractional rms amplitude than any of the kHz QPOs seen during the Z phase, and that in the same frequency range, atoll lower kHz QPOs show coherence and fractional rms amplitude, respectively, two and three times larger than the Z kHz QPOs. Out of the 707 observations in the Z phase, there is no single observation in which the kHz QPOs have a coherence or rms amplitude similar to those seen when XTE J1701−462 was in the atoll phase, even though the total exposure time was about five times longer in the Z than in the atoll phase. Since it is observed in the same source, the difference in QPO coherence and rms amplitude between the Z and atoll phase cannot be due to neutron star mass, magnetic field, spin, inclination of the accretion disc, etc. If the QPO frequency is a function of the radius in the accretion disc in which it is produced, our results suggest that in XTE J1701−462 the coherence and rms amplitude are not uniquely related to this radius. Here we argue that this difference is instead due to a change in the properties of the accretion flow around the neutron star. Regardless of the precise mechanism, our result shows that effects other than the geometry of space–time around the neutron star have a strong influence on the coherence and rms amplitude of the kHz QPOs, and therefore the coherence and rms amplitude of the kHz QPOs cannot be simply used to deduce the existence of the innermost stable circular orbit around a neutron star.

Key words: accretion, accretion discs – stars: neutron – X-rays: binaries – X-rays: individual: XTE J1701−462.

1 INTRODUCTION

It is now more than 13 yr ago that kilohertz quasi-periodic oscillations (kHz QPOs) were discovered (Strohmayer et al. 1996; van der Klis et al. 1996) in neutron star (NS) low-mass X-ray binary (LMXB) systems. Interest in this phenomenon remains high

⋆E-mail: a.sanna@astro.rug.nl

because of the close correspondence between kHz QPO time-scales and typical dynamical time-scales of matter orbiting close to an NS. For this reason, kHz QPOs are potential tools to probe general relativity in the strong gravitational field regime (van der Klis 2005), and constrain the NS equation of state (Miller, Lamb & Cook 1998a).

Since the launch of the *Rossi X-Ray Timing Explorer* (*RXTE*) in 1995, kHz QPOs have been detected in about 30 NS LMXBs (for a review see van der Klis 2005). Most of these sources show two simultaneous kHz QPOs, usually called the lower and the upper kHz QPO, with frequencies that can drift as a function of time in the range 250–1200 Hz (van der Klis 2006). Studies of these kHz QPOs show that QPO frequencies are related to other properties of the source; e.g. on short time-scales (within a day or less) QPO frequencies are well correlated with the intensity of the source, whereas on long time-scales this correlation breaks down and intensity–frequency diagrams show the so-called 'parallel tracks' (Méndez et al. 1999). The frequencies of the kHz QPOs correlate also with the position of the source in the colour–colour diagram, and with parameters of spectral components used to describe the X-ray spectrum of these sources (Wijnands et al. 1997; Kaaret et al. 1999; Méndez & van der Klis 1999; Di Salvo et al. 2001). Nevertheless, it is still unclear which physical parameters drive the QPO frequency, although there are indications that mass accretion rate, $\dot{m}$, plays a key role (Miller et al. 1998a).

Several models have been proposed to explain the kHz QPOs (e.g. Miller, Lamb & Psaltis 1998b; Stella & Vetri 1998; Abramowicz et al. 2003), as well as the connection between high-frequency QPOs and other time variability usually present in power-density spectra (for a review of variability at low frequencies see van der Klis 2001). Despite these efforts, there is still no single model that is able to explain in a self-consistent way all the QPO properties.

kHz QPOs are characterized by three parameters: centroid frequency ν, quality factor $Q = \nu/\mathrm{FWHM}$, where FWHM is the full width at half-maximum of the QPO, and fractional rms amplitude. Systematic analyses of these kHz QPO properties have been done for a large number of sources (e.g. Jonker et al. 2000; van Straaten et al. 2000; Di Salvo et al. 2001; Méndez, van der Klis & Ford 2001; Homan et al. 2002; van Straaten et al. 2002; Di Salvo, Méndez & van der Klis 2003; Altamirano et al. 2005; Barret et al. 2005a; Barret, Olive & Miller 2005b, 2006; Méndez 2006). Those studies show that, in each source the quality factor and the rms amplitude of the lower kHz QPO increase with the centroid frequency of the QPO until they reach a maximum value, after which they decrease as the frequency continues to increase (e.g. Méndez et al. 2001; Di Salvo et al. 2003; Barret et al. 2005b; see Méndez 2006 for a compilation of results). The upper kHz QPO does not show the same trend; in this case the quality factor usually does not change with the centroid frequency while the rms amplitude stays more or less constant at lower frequencies and then decreases as the frequency increases (van Straaten et al. 2002; van Straaten, van der Klis & Méndez 2003; Barret et al. 2005a; Altamirano et al. 2008).

Barret et al. (2005b) and Barret et al. (2006) interpreted the drop of the quality factor of the lower kHz QPO at high frequencies in the LMXBs 4U 1636−536 and 4U 1608−522 as a signature of the inner disc radius reaching the innermost stable circular orbit (ISCO), and starting from that assumption they estimated the mass and the radius of the compact object in these two systems. However, Méndez (2006) argued against this idea and suggested that the drop of Q and rms in individual sources might be related (at least in part) to changes of the properties of the accretion flow in these systems.

Following those results, here we investigate the properties of the kHz QPOs for the transient NS LMXB XTE J1701−462. This source was detected for the first time on 2006 January 18 with the all-sky monitor on board *RXTE* (Remillard et al. 2006). As reported by Homan et al. (2007a), Lin, Remillard & Homan (2009a), Aresu & Sanna (in preparation) and Homan et al. (2010), this is the only source so far that showed both Z and atoll behaviour (for more details about the Z and atoll classes see Hasinger & van der Klis 1989). The luminosity range covered by XTE J1701−462, from Eddington limit to quiescence, gives us a unique opportunity to study kHz QPO properties in different states and, more importantly, at different mass accretion rates in the same system, which could provide vital information to understand the origin and the mechanisms that drive the properties of these QPOs.

In Section 2 we describe the observations and the data analysis, and in Section 3 we present our results. In Section 4 we discuss those results in the context of current ideas concerning the mechanisms behind the kHz QPOs in LMXBs, and in Section 5 we summarize our conclusions.

2 OBSERVATIONS AND DATA ANALYSIS

We analysed all the public data of the LMXB XTE J1701−462 collected with the Proportional Counter Array (PCA) on board of *RXTE* (Bradt, Rothschild & Swank 1993; Jahoda et al. 2006). There are 866 observations of this source in the *RXTE* archive, for a total exposure time of ∼3 Ms. During these observations the source showed several type I X-ray bursts that we excluded from our analysis (see Lin et al. 2009b for a detailed analysis of the bursts).

2.1 Timing analysis

To search for kHz QPOs, we created Leahy-normalized power-density spectra using event-mode data with 125 μs time resolution covering the full PCA energy band, nominally from 2 to 60 keV. We created Fourier power-density spectra from 16-s data segments, using 1/4096 s time resolution such that the frequency range is defined from 0.0625 to 2048 Hz. We removed detector dropouts; no dead-time correction or subtraction of background contribution was done to calculate the power-density spectra. We created one averaged power-density spectrum for each observation that we visually inspected to search for the presence of QPOs with characteristic frequencies in the range from 200 to 1200 Hz. We found kHz QPOs in 14 out of the 866 observations that we analysed.

Following Aresu & Sanna (in preparation) and Homan et al. (2010), we considered that XTE J1701−462 was in the Z phase from its discovery in 2006 January (Remillard et al. 2006) until the end of 2007 April [as reported by Aresu & Sanna (in preparation) and Homan et al. (2010), no clear boundary between Z and atoll phase has been found which makes this date just an approximation], when it started to behave as an atoll source until it went into a quiescence state. Using this division, there are 707 observations (∼2.5 Ms) of XTE J1701−462 in the Z phase and 159 observations (∼0.5 Ms) in the atoll phase. kHz QPOs were detected in individual observations only in the horizontal branch during the Z phase and in the lower banana in the atoll phase of the outburst (see Homan et al. 2010). From 14 observations with kHz QPOs, eight belong to the Z phase (ObsIDs are reported in Table 1) and six to the atoll phase (observations 93703-01-02-04, 93703-01-02-11, 93703-01-02-05, 93703-01-02-08, 93703-01-03-00 and 93703-01-03-02).

Table 1. Properties of the kHz QPOs detected in the Z phase of XTE J1701−462. Subscript letters u and l denote upper and lower kHz QPOs, respectively. Parameters without errors represent 95 per cent confidence level upper limits. All other errors reported represent 1σ confidence intervals.

ObsID	Z phase					
	L_l			L_u		
	Q_l	rms_l per cent	ν_l (Hz)	Q_u	rms_u per cent	ν_u (Hz)
91442-01-07-09	35.3 ± 18.8	1.4 ± 0.2	642.7 ± 3.1	52.8 ± 38.8^a	< 1.6	932.6 ± 7.9^a
92405-01-01-02	22.6 ± 11.1	3.4 ± 0.5	615.1 ± 3.8	56.9 ± 28.8	2.9 ± 0.5	944.9 ± 3.7
92405-01-01-04	5.4 ± 2.8^a	< 3.5	502.4 ± 23.1^a	10 ± 3	3.1 ± 0.3	760.8 ± 6.4
92405-01-02-03	11.9 ± 6.5	3.0 ± 0.5	623.9 ± 8.3	20.6 ± 11.1	2.7 ± 0.4	911.2 ± 8.4
92405-01-02-05	8.9 ± 6.9	2.7 ± 0.4	595.9 ± 10.1	6.2 ± 1.4	4.1 ± 0.4	850.5 ± 12.4
92405-01-03-05	8.5 ± 2.7	4.6 ± 0.5	612.5 ± 7.7	10.5 ± 3.5	4.6 ± 0.6	917.3 ± 10.6
92405-01-40-04	9.2 ± 3.2	2.8 ± 0.3	650.5 ± 7.1	11.1 ± 3.1	2.9 ± 0.3	911.0 ± 8.6
92405-01-40-05	8.1 ± 2.4	3.0 ± 0.3	637.9 ± 8.6	12.9 ± 3.5	3.0 ± 0.3	919.8 ± 7.6

[a]These parameters are calculated for kHz QPOs with a significance level lower than 3σ (see the text for precise values).

A quick analysis of the observations showed clear differences in the properties of the QPOs between Z and atoll phases (see Section 3 for a detailed discussion). The QPOs were always weaker and broader in the Z than in the atoll phase. It is well known that the frequency of the kHz QPOs can change over tens of Hz in time intervals of a few hundred seconds (e.g. Berger et al. 1996), and this can artificially broaden the QPO in the averaged power spectrum of long observations. Therefore, for each observation in which we found a kHz QPO, we divided the observation in smaller intervals to check if a significant QPO was still present, and whether the QPO frequency was changing. We found that in the Z phase it was not possible to detect a significant kHz QPO in power spectra of intervals shorter than a full observation: in all observations in the Z phase with kHz QPOs the QPOs were weak and broad over short time intervals. Therefore, for the rest of the analysis, for the Z phase we report QPO properties for the average power-density spectrum of each observation. In the atoll phase, the kHz QPOs were significantly detected on time intervals shorter than a full observation, and in most cases the frequency was changing in time. Therefore, for the atoll phase, we decided to average power-density spectra according to the frequency of the QPO. To do this we produced power-density spectra of 16 s of data, and averaged up to 15 of these power spectra to get a significant detection of the kHz QPO from which we measured the QPO frequency as a function of time. Finally we averaged power-density spectra such that the frequency of the QPO was within a range of 10–60 Hz (frequency intervals are reported in Table 2). We shifted the frequency scale of all these power-density spectra in order to align the frequencies of the QPOs to a constant value and then averaged the power-density spectra to create one power-density spectrum per selection (see Méndez et al. 1998). We fitted each Z and atoll average power-density spectrum in the frequency range 200–1200 Hz using a constant to model the Poisson noise plus one Lorentzian to model the kHz QPO. It must be clarified that, for the atoll phase, the centroid frequencies of the QPOs reported in Table 2 are the mean frequencies within the interval selected, and the errors associated are the standard deviations of the selection.

Table 2. Properties of the kHz QPOs detected in the atoll phase of XTE J1701−462. Column 2 shows the frequency selections used to create the intervals (see text for details). Columns 3–5 show the quality factor, the fractional rms amplitude and the frequencies of the kHz QPOs, respectively. All errors represent 1σ confidence intervals.

Interval	Hz	Atoll phase		
		Q	rms per cent	ν (Hz)
1	600–660	69.9 ± 17.1	9.8 ± 0.9	640.9 ± 13.5
2	660–700	59.6 ± 15.6	10 ± 1	673.3 ± 14.5
3	700–750	98.2 ± 14.8	9.2 ± 0.5	716.8 ± 6.7
4	750–780	67.1 ± 19.2	11.8 ± 1.2	772.2 ± 4.2
5	780–800	106.9 ± 9.7	9.9 ± 0.3	793.9 ± 5.4
6	800–820	150.3 ± 20.9	8.7 ± 0.4	811.5 ± 6.6
7	820–830	114.9 ± 12.7	9.3 ± 0.4	827.3 ± 2.6
8	830–840	93.4 ± 8.7	8.9 ± 0.3	835.8 ± 2.6
9	840–850	100.6 ± 13.9	7.9 ± 0.4	846.2 ± 2.9
10	850–950	123.9 ± 36.8	6.6 ± 0.7	854.8 ± 4.3

In order to label the QPOs we used the standard convention introduced by Belloni, Psaltis & van der Klis (2002) where each QPO is denoted with the letter L with a subscript that specifies the category. In this particular case we were interested in kHz QPOs so we used L_l and L_u to identify the lower and the upper kHz QPO, respectively. Following this criterion all the characteristics associated with one QPO have the same label.

We estimated the fractional rms amplitude of QPOs in the atoll phase in different energy bands. For each observation with QPOs we first created power-density spectra in five different energy intervals: 2–3, 3–6, 6–11, 11–16 and 16–25 keV (we stopped at 25 keV because of the lack of sensitivity of the detector above that energy). We shifted and added the power-density spectra creating one single power-density spectrum for each energy band and we fitted these power-density spectra as the atoll power-density spectra previously described. To calculate the fractional rms amplitude we calculated the integral power of the Lorentzian and we renormalized it using the source and background count rate (see van der Klis 1997).

2.2 Spectral analysis

We calculated X-ray colours and intensity of the source using the Standard 2 mode data. We defined a hard colour as the count rate ratio in the energy bands 9.7–16.0 and 6.0–9.7 keV, and the intensity of the source as the count rate in the energy band 2.0–16.0 keV. To obtain the exact count rate in each of these bands we interpolated in channel space. To correct for the gain changes and differences in the effective area between the proportional counter units (PCUs) as well as differences due to changes in the channel to energy conversion of the PCUs as a function of time, we normalized our colour and intensity by the Crab nebula values obtained close in time to our observations and per PCU (see Kuulkers et al. 1994; Altamirano et al. 2008 for details). Finally we averaged the normalized colours and intensities per PCU every 16 s using all available PCUs.

We also calculated the source luminosity for all 14 observations containing kHz QPOs. In order to do so, we first created a light

curve for each observation, we then checked for X-ray bursts and detector dropouts, and if any were present we eventually excluded them from the analysis. Using Standard 2 data we extracted energy spectra following the procedures described in the *RXTE* web page, and we added a 0.6 per cent systematic error in quadrature to each channel. We fitted the energy spectra in XSPEC in the energy range from 3 to 22 keV using a model consisting of a blackbody and a multicolour blackbody for the Z observations, while we added also a broken power law with the break energy fixed at 20 keV to fit the atoll observations (see Lin et al. 2009a). These models also include absorption from the interstellar medium towards the source and when necessary we added a Gaussian emission line at ∼6.5 keV. The reduced χ^2 of our fits range from 0.6 to 1.1 (for 36 d.o.f.). From the best-fitting model we calculated the unabsorbed flux in the energy range 2–50 keV, setting the $N_{\rm H}$ to zero and creating an artificial response function for the full energy range 2–50 keV. We then estimated the luminosity assuming a distance $d = 8.8$ kpc (Lin et al. 2009b).

3 RESULTS

In Tables 1 and 2 we report the quality factor Q, fractional rms amplitude and frequency of the kHz QPOs detected in all the *RXTE* observations available for XTE J1701−462, from 2006 January to 2007 August.

In Table 1 we show the properties of the kHz QPOs during the Z phase. The significance level of these QPOs ranges between 3.2σ and 6σ, except for $L_{\rm u}$ in observation 91442-01-07-09 and $L_{\rm l}$ in observation 92405-01-01-04 which have, respectively, significances of 2.4σ and 2.3σ. [The significances of kHz QPOs are given as the ratio of the integral of the power of the Lorentzian used to fit the QPO divided by the negative error of the power. As shown by Boutelier et al. (2010), this probably underestimates the true significance of the QPOs.] For these two kHz QPOs we report upper limits. During the Z phase the lower and upper kHz QPOs show similar quality factors, on average around 15; also the fractional rms amplitude of the two QPOs is similar, between ∼1.4 and 4.5 per cent.

In Table 2 we report the properties of the 10 QPOs detected in the frequency-selected intervals in the atoll phase. These QPOs have significances between 5σ and 15σ. The QPO frequency varies from 640 to 860 Hz; the quality factor changes from about 60 up to 150. The fractional rms amplitude ranges from about 7 to 12 per cent.

3.1 QPO identification

While for the Z phase it is easy to label the QPOs, for the atoll phase the identification is not straightforward since there we found just one QPO in each observation. A quick inspection of the values in Table 2 shows similar QPO properties between different intervals, which indicate that in all cases we are probably dealing with the same QPO. To progress further we compared Q and rms values with those of other LMXBs where two simultaneous kHz QPOs have been studied (Wijnands et al. 1997; Jonker et al. 1998; Wijnands et al. 1998; Barret et al. 2005a; Barret et al. 2005b, 2006); the coherence and rms amplitude are similar to those of the lower kHz QPO in other atoll sources.

According to Belloni et al. (2007) and Méndez et al. (1999), lower and upper kHz QPOs in atoll sources follow two different tracks in the frequency-hardness diagram. Lower kHz QPOs are found when the source has low hard colour and the centroid frequency does not seem to be correlated with hard colour (as the frequency changes the hard colour changes slightly in a restricted range). On the contrary, upper kHz QPOs are found where the source has high hard colour that decreases as the QPO frequency increases (see fig. 3 in Belloni et al. 2007). In Fig. 1 we plot the QPO frequency as a function of the hard colour and intensity of the source. All points are concentrated within a narrow hard colour range, from 0.7 to 0.75, while the frequency ranges from 640 to 860 Hz. The fact that the hard colour changes within a restricted range while the frequency moves in a range of about 200 Hz resembles what Belloni et al. (2007) show concerning the lower kHz QPO behaviour in the atoll source 4U 1636−53. This further supports our identification of the kHz QPOs in the atoll phase as lower kHz QPOs.

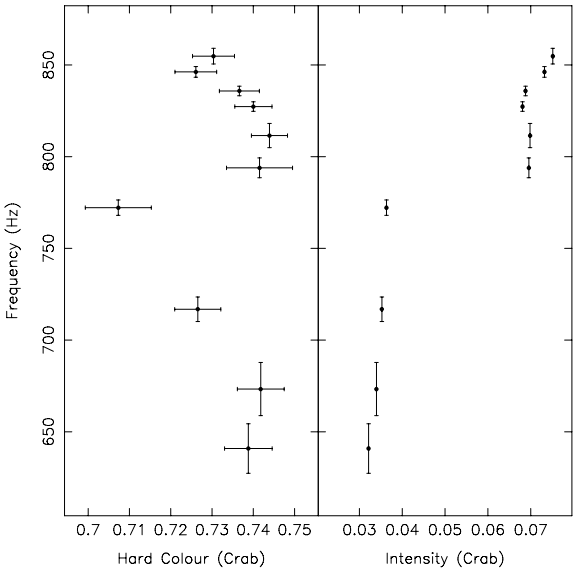

Figure 1. Left-hand panel shows the frequency of the QPOs in the atoll phase of XTE J1701−462 as a function of the hard colour of the source. Right-hand panel shows the frequency of the QPOs as a function of the intensity of the source.

In order to understand the frequency-hardness diagram, we plot in the right-hand panel of Fig. 1 the QPO frequency as a function of the source intensity. It is apparent from the graph that the data are divided into two different tracks characterized by intensity values which differ by a factor of ∼2. That trend resembles the so-called 'parallel tracks' phenomenon which has been seen in many LMXBs (see e.g. Méndez et al. 1999). Although the points in Fig. 1 are the result of frequency selection, it turns out that all the QPOs we combined to make the intervals from 1 to 4 and from 5 to 10 in Table 2 are concentrated in a time interval, respectively, of about 1 d and less than half a day. Moreover, those two groups are separated by more or less 4 d, which means the points in the right-hand panel of Fig. 1 can in fact reflect the 'parallel tracks' phenomenon.

We note that QPOs at the highest intensities correspond to the ones with the highest frequencies in the frequency-hardness diagram, while QPOs at the lowest intensities correspond to those with the lowest frequencies in the frequency-hardness diagram. This can be interpreted as 'parallel tracks' in the frequency-hardness diagram. A similar trend was seen in the LMXB 4U 1636−53 (see fig. 2 in Di Salvo et al. 2003).

To search for a second (possibly weaker) kHz QPO in the atoll phase we apply the shift-and-add method (Méndez et al. 1998). As we described in Section 2, first we fit the centroid frequency of the kHz QPO in each individual atoll power-density spectrum, then we shift all the power spectra such that the kHz QPO frequencies are aligned at the same value. Finally we average all the data into

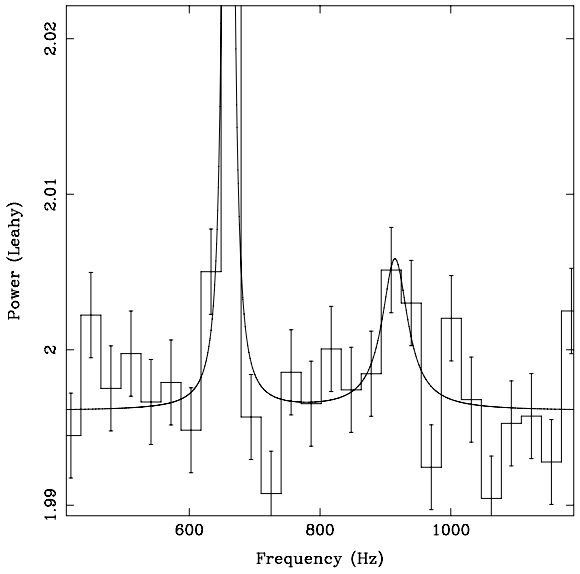

Figure 2. Power-density spectrum of all the atoll observations where QPOs are detected. This power spectrum is the result of the shift-and-add method. Two kHz QPOs are visible, the one at lower frequency (30σ significant) was the one originally used to shift and add the power spectra, while the one at higher frequencies (3.1σ significant, single trial) appears as result of the application of the method.

a single power-density spectrum which we fit with a constant plus Lorentzian component for each QPO. This method corrects the frequency drift in time of the kHz QPOs, increasing their signal-to-noise ratio and their significance. If the second kHz QPO is at a (more or less) fixed distance from the first, this method adds all the data in a way that increases the significance of the second QPO, which may then become detectable.

The result of this procedure is presented in Fig. 2, which shows two simultaneous kHz QPOs, the one at lower frequency is the kHz QPO which we already knew, while the second one becomes detectable as a result of the shift-and-add method. The significance level of the second, upper, kHz QPO is 3.1σ, which implies a marginal detection. Note however that the frequency difference between the kHz QPOs is 258 ± 13 Hz, which is consistent with the value in the Z phase (see Table 1 and Homan et al. 2007b) and therefore there are no other trials involved in estimating this significance. As a result of this analysis, taking into account all the caveats, we find a pair of simultaneous kHz QPOs in the atoll phase of the XTE J1701−462 which strengthens our previous suggestion that the strong kHz QPOs detected in this phase are always the lower kHz QPO.

As described in Section 2, we calculate the fractional rms amplitude of the atoll QPOs in five different energy bands, 2–3, 3–6, 6–11, 11–16 and 16–25 keV, respectively. We find fractional rms amplitudes of less than 10.9 per cent, $6.9 \pm 0.3, 11.4 \pm 0.2$, 17.5 ± 1.2 and less than 21.3 per cent, respectively (upper limits are given at 95 per cent confidence). Those results, as already noted in other sources (see Berger et al. 1996), show that the strength of the variability increases as the energy increases.

3.2 Amplitude and coherence of the kHz QPOs in the Z and atoll phases

Fig. 3 shows the values of the QPO quality factor as a function of frequency. Black points represent measurements in the atoll phase while grey points are measurements in the Z phase. For the Z phase, empty and filled square symbols represent, respectively, lower and upper kHz QPOs. From the plot we note a few interesting aspects. (1) QPOs in the atoll phase are on average 10 times more coherent than in the Z phase. (2) In the atoll phase Q increases as the frequency increases, reaching a maximum value of about 150 at ∼810 Hz; within the errors the behaviour is consistent with what has been observed in other sources (see Barret et al. 2005a). No such trend seems to be present in the Z phase. (3) Comparing lower kHz QPOs in both phases it is clear that in the Z phase the lower kHz QPO

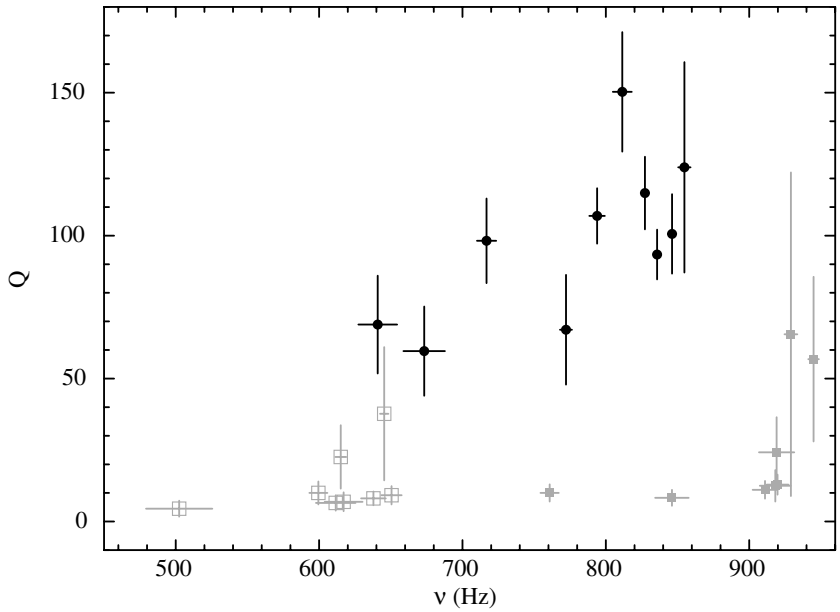

Figure 3. Quality factor Q as a function of the QPO centroid frequency for XTE J1701−462. Black points represent QPOs in the atoll phase, and grey points represent QPOs in the Z phase. Empty and filled squares indicate lower and upper kHz QPOs, respectively. The values of the coherence at frequencies ∼500 Hz, ∼615 Hz, ∼930 Hz and ∼940 Hz correspond to kHz QPOs with significances 2.8σ, 2.1σ, 2.4σ and 2σ, respectively (see text).

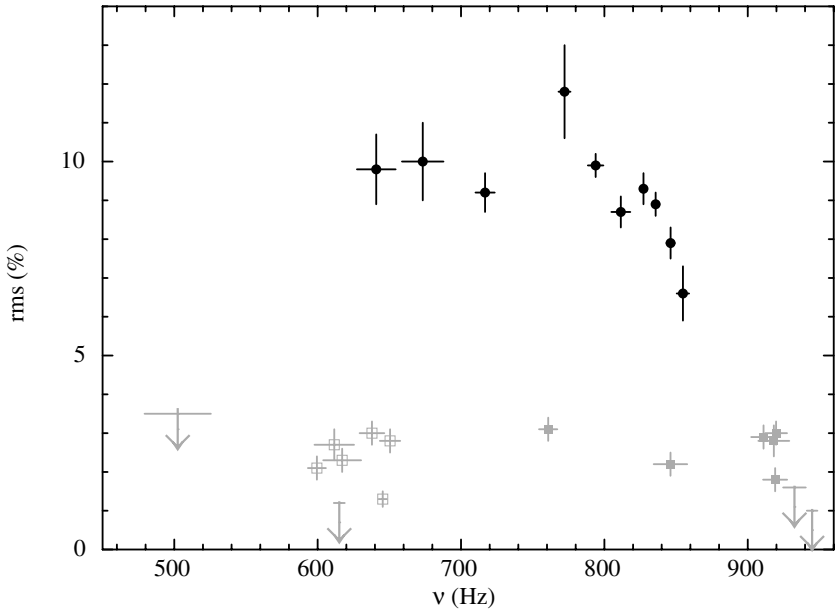

Figure 4. Factional rms amplitude as a function of the QPO centroid frequency for XTE J1701−462. Black points represent QPOs in the atoll phase, and grey points represent QPOs in the Z phase. Empty and filled squares indicate lower and upper kHz QPOs, respectively. Arrows correspond to 95 per cent confidence level upper limits.

appears at lower frequencies than in the atoll phase. (4) There is an overlap in frequency around 640 Hz between Z and atoll QPOs with a significant mismatch in Q.

Fig. 4 shows the QPO rms fractional amplitude as a function of frequency. As in Fig. 3, black points denote measurements in the atoll phase, while grey points are QPOs in the Z phase. The rms amplitude of the lower kHz QPO in the atoll phase remains more or less constant around 10 per cent as the QPO frequency increases from 640 to 780 Hz and then drops rapidly at ∼800 Hz. There is no evidence of a similar trend for the rms of the lower or upper kHz QPOs in the Z phase. As already noted for the quality factor, the rms amplitude values show a clear difference between the atoll and Z phases: the lower kHz QPOs amplitude in the atoll phase is on average a factor of 2 higher than in the Z phase; this difference is also apparent in the region where atoll and Z QPOs overlap in frequency between 620 and 660 Hz.

We test whether we may have missed any significant kHz QPO in our analysis. We calculate upper limits to the fractional rms amplitude in frequency ranges where we did not find kHz QPOs. To do so we take two power-density spectra, one for each source phase, where no kHz QPOs were found. We fit those power-density spectra using a model consisting of a constant to fit the Poissonian noise and a Lorentzian to fit the QPO with fixed values for the centroid frequency and the quality factor Q. We fit the data and estimate the upper limit of the amplitude of the Lorentzian using $\Delta\chi^2 = 2.7$, which corresponds to 95 per cent confidence level. We repeat the same procedure shifting gradually the frequency of the Lorentzian to higher values until we cover the frequency range of interest.

For the analysis of atoll observation we use power-density spectra of 256 s, comparable to the time intervals over which we detected kHz QPOs in the atoll phase. We use two different quality factors, $Q = 50$ and 20, which are comparable to the values we found for the kHz QPOs at low frequencies (see Table 2). We find upper limits to the fractional rms amplitude that vary within the range 2.7–5.2 per cent and within the range 3–7 per cent, respectively, for $Q = 20$ and 50. From these values it appears that the rms amplitude of the lower kHz QPO in the atoll phase should decrease at frequencies lower than 640 Hz. This would be in agreement with the typical rms-frequency trend observed in most of the LMXBs (van Straaten et al. 2000; Di Salvo et al. 2001; Méndez et al. 2001; van Straaten et al. 2002; Di Salvo et al. 2003; van Straaten et al. 2003; Barret et al. 2005a).

For the Z observation, we estimate the upper limits to the amplitude of a kHz QPO with typical atoll properties within short time intervals to check whether we could have missed such a QPO during the analysis. We calculate the upper limits in the frequency range 650–940 Hz assuming a kHz QPO with $Q = 100$ and setting three values of the integration time, 128, 256 and 512 s. We find that the upper limits to the fractional rms amplitude vary between 1 and 4 per cent for 128 s of integration time, between 0.8 and 4 per cent for 256 s and between 0.4 and 3.4 per cent for 512 s. From this we conclude that if a kHz QPO with $Q = 100$ and fractional rms amplitude similar to what we found for the atoll kHz QPOs was present in the Z observations, we would have detected it significantly in intervals as short as 128 s.

4 DISCUSSION

The transient source XTE J1701−462 is so far the only accreting NS X-ray binary that changed from a Z into an atoll source during an outburst. Here we found that the properties of the kHz QPOs in XTE J1701−462 in the atoll and Z phases are significantly different: at approximately the same frequency (about 640 Hz), the coherence of the kHz QPOs is a factor of 2 larger, and the rms amplitude is a factor of 3 larger, in the atoll than in the Z phase (see Figs 3 and 4, respectively). Furthermore, out of 707 observations in the Z phase, there is no single observation in which the kHz QPOs have a coherence or rms amplitude similar to those seen when XTE J1701−462 was in the atoll phase, even though the total exposure time was about five times longer in the Z than in the atoll phase. If the kHz QPOs reflect the motion of matter in the accretion disc, and the QPO centroid frequency is related to the radius in the accretion

disc where this motion takes place, our results show that, at least in XTE J1701−462, there is no unique relation between the radius of the disc at which the QPO is produced and the coherence and rms amplitude of the QPO.

It was already known that the kHz QPOs are broader and weaker in Z than in atoll sources (see Méndez 2006 for a compilation), but this is the first time that the same trend is observed in a single source. This result conclusively excludes things like NS mass, magnetic field, spin, inclination of the accretion disc, etc., as the cause of this trend since these parameters cannot change on time-scales of one and half years. As we discuss below, the most likely reason for the difference of QPO coherence and rms amplitude between the Z and atoll phase in XTE J1701−462 is a change in the properties of the accretion flow around the NS where the QPOs are produced. Despite the lack of information about the precise mechanism, our result shows that effects other than the geometry of space–time around the NS have a strong effect on the QPO properties. If, as suggested by Barret et al. (2005a) and Barret, Olive & Miller (2005c), the ISCO affects the coherence and rms amplitude of the kHz QPOs, our result shows that there are other mechanisms that should also be taken into account to explain the trend seen in the data. For instance, in XTE J1701−462 the coherence and rms amplitude differ by a factor of ∼3–10 between the Z and atoll phases similar, for instance, to the change of coherence and rms amplitude that has been proposed to be due to the ISCO in 4U 1636−53 (Barret et al. 2005b).

Méndez (2006) found that the behaviour of the coherence and rms amplitude of the kHz QPOs in individual sources is similar to the behaviour of the maximum coherence and maximum rms of the kHz QPOs as a function of the luminosity in a sample of 12 NS LMXBs. It is interesting to test to what extent this luminosity relation holds for the Z and atoll phases of XTE J1701−462, which are well separated in luminosity. In Fig. 5 we combine the data points from the Z and atoll phases of XTE J1701−462 with those of the 12 NS LMXBs studied by Méndez (2006).

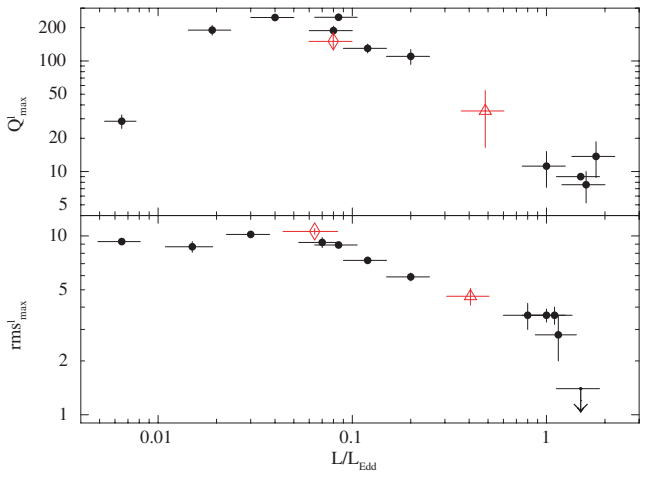

Figure 5. Upper panel: the maximum fractional rms amplitude of the lower kHz QPO for a sample of 12 sources (filled circles, see table 1 of Méndez 2006 for the source names) plus XTE J1701−462 as a function of the luminosity of the source. The diamond and the triangle represent, respectively, measurements in the atoll and the Z phase. Lower panel: the maximum quality factor of the lower kHz QPO for the same sources mentioned above as a function of the luminosity of the source. The symbols are the same as in the upper panel. The luminosity is in units of the Eddington luminosity for a 1.9 $M_\odot$ NS.

The upper and the lower panels show, respectively, the maximum quality factor and the maximum rms amplitude of the lower kHz QPO for 13 sources as a function of the luminosity of the source in the 2–50 keV range, normalized by the Eddington luminosity, $L_{Edd} = 2.5 \times 10^{38}$ erg s^{-1}, corresponding to a NS of 1.9 $M_\odot$ accreting gas with cosmic abundance. As it is apparent from the plots, XTE J1701−462 follows the trends already traced by the other sources; moreover the coherence of the kHz QPOs in the Z phase fill the gap between the atoll sources in the left-hand side and the Z sources in the right-hand side of the graph, strengthening the correlation. (Note, however, that the luminosity of XTE J1701−462 could be uncertain by up to a factor of ∼2; Lin et al. 2009a.)

Besides differences of the kHz QPOs properties between Z and atoll sources, Fig. 5 shows also a trend of both Q and rms amplitude within the atoll sources. This is noticeable in the lower panel of fig. 5 of Méndez (2006), where the maximum coherence and maximum rms amplitude of the lower kHz QPO are plotted versus each other. From that plot it is apparent that the two quantities both in Z and atoll sources follow the same correlation (see Méndez 2006). This suggests that there is a single mechanism behind this trend. Our observations of XTE J170−462 in the Z and atoll phase are in line with this.

We can qualitatively explain how it is possible to find high rms amplitudes of kHz QPOs at energies where the contribution of the disc is insignificant. As reported by Berger et al. (1996), the rms amplitude of the lower kHz QPO in the LMXB 4U 1608−52 increases with energy up to 20 per cent (fraction of the total emitted flux) at energies around 30 keV, significantly above the energy range where the accretion disc contributes to the X-ray spectrum (see also Méndez et al. 2001; Gilfanov, Revnivtsev & Molkov 2003; Altamirano et al. 2008). If the kHz QPOs are produced in the accretion disc, this must imply the presence of a mechanism that amplifies the variability at different energy bands. Some mechanisms have been proposed for this: Lee & Miller (1998) found that oscillations of the density and temperature of the Comptonizing medium can reproduce the rms amplitude behaviour of the lower kHz QPO in the atoll source 4U 1608−52. Gilfanov et al. (2003), from the analysis of the Z source GX340+0, suggest that QPOs are related to the contribution of the boundary-layer emission to the total source emission. Gilfanov & Revnivtsev (2005) found that as $\dot{m}$ increases from the horizontal branch to the flaring branch along the Z-shaped track in the colour–colour diagram of GX 340+0, the contribution of the boundary layer decreases. If we combine the results of Gilfanov et al. (2003) and Gilfanov & Revnivtsev (2005), and we apply them to the case of XTE J1701−462, we would expect the boundary-layer contribution to be stronger in the atoll phase than in the Z phase. To verify this, we used the spectral analysis of XTE J1701−462 done by Lin et al. (2009a); their figs 14 and 15 show the spectral fitting results, respectively, of the atoll and the Z phase. From their fig. 14 we note that in the atoll phase the blackbody (BB) component used by Lin et al. (2009a) to fit the boundary-layer emission becomes dominant, while the emission from the disc (fitted with a multicolour disc BB) becomes negligible. Comparing this with their fig. 15, we found that the fractional contribution of the boundary-layer emission in the atoll phase is higher than in the Z phase, which is in agreement with the results of Gilfanov et al. (2003), and can also explain the fact that we found stronger kHz QPOs in the atoll phase than in the Z phase. If this is correct, we should expect that most of the variability concentrates in the energy band where the boundary-layer emission peaks. From fig. 14 of Lin et al. (2009a), the BB temperature is about 2 keV, which implies

that the peak of the boundary-layer emission is at about 10 keV. According to the results shown in the previous section, the atoll fractional rms amplitude increases as the energy increases, up to about 20 per cent in the energy band 16–25 keV. We test whether the fractional rms amplitude we found above 10 keV is compatible with the fractional contribution of the boundary-layer emission to the total emission of the source. From the spectral fits shown by Lin et al. (2009a, see their fig. 12 panel 'atoll SS'), the BB contributes more than 30 per cent of the total emission in the 10–25 keV band, which means that the picture where the amplitude and coherence of the kHz QPOs are driven by the boundary layer is still consistent at those energies. Further studies should address the fact the kHz QPOs are only detected over narrow regions in the colour–colour diagram.

Adding all these together, we suggest a possible scenario to describe the behaviour of the properties of the kHz QPO. Mathematically a Lorentzian (which is usually used to model quasi-periodic oscillations) is the Fourier transform of an exponentially damped sinusoid signal, $A\,\mathrm{e}^{-t/\tau}\,\sin(2\pi\nu t+\phi)$, where A is the amplitude of the signal, τ is the lifetime of the variability, ν is the frequency of the oscillation and ϕ is an arbitrary phase. Starting from this mathematical expression we can build a qualitative mechanism to describe the behaviour of the quality factor and the rms of the kHz QPO. Most of the models proposed to explain the kHz QPOs consider the disc as the most probable location where those QPOs are generated (e.g. Miller et al. 1998b). Under this assumption, the above expression could represent the oscillator that generates the QPO in the disc and sets its frequency ν. Since the rms amplitude of kHz QPOs depends on energy, we should introduce an energy-dependent amplification factor $B(E)$ which should be physically related to the mechanism which generates high-energy photons. For example, this could be related to the properties of the Comptonizing medium (Lee & Miller 1998) or to the contribution of the boundary-layer emission to the total emission of the source (Gilfanov et al. 2003; Gilfanov & Revnivtsev 2005). The parameter τ determines the QPO width, and as in the case of the amplitude, it also could be energy dependent. Additionally, we should consider that each process that amplifies the variability could also modify the lifetime of the variability. Just to give an example, if the QPO is created in the disc, and later on the QPO photons interact with matter in the corona, the final width of the QPO will be the result from the combination of the two processes. In our model this would imply a lifetime for the QPO $1/\tau_{\rm tot} = (\tau_{\rm disc} + \tau_{\rm cor})/(\tau_{\rm disc}\,\tau_{\rm cor})$. With these considerations, the modulated flux in the kHz QPO could be described by the expression $B(E)A\,\mathrm{e}^{-t/\tau_{\rm tot}}\,\sin(2\pi\nu t+\phi)$. This simple expression describes the rms amplitude and coherence of the QPO in terms of the quantities $B(E)$ and $\tau_{\rm tot}$, which in turn could depend on the properties of the boundary layer. The above expression would reproduce the behaviour of the rms amplitude and coherence if, for instance, $B(E)$ and $\tau_{\rm tot}$ depended upon mass accretion rate, $\dot{m}$, such that $B(E)$ and $\tau_{\rm tot}$ decreased as $\dot{m}$ increased. The previous description does not resolve however the issue of which processes are involved, or what the key mechanisms are that create or amplify the QPO signal. Nevertheless, this qualitative explanation provides a starting point to build a realistic model to explain the kHz QPO properties.

For most of the considerations in this paper we assumed that the only kHz QPO in the atoll phase is the lower kHz QPO. Although it is very unlikely (see Section 3), if it instead was the upper kHz QPO, one would have to explain the fact that in the frequency range, from 740 to 860 Hz, the atoll kHz QPOs show Q and rms values significantly different than those of the Z phase kHz QPOs (Figs 3 and 4).

From the *INTEGRAL* catalogue (*INTEGRAL* general reference catalogue, Version 30) we found no other sources within 1 deg^2 of the position of XTE J1701−462. The closest source reported (about 2.°3 away from XTE J1701−462) is the gamma-ray source 2EGS J1653−4604 that does not show X-ray emission. Krauss et al. (2006) observed XTE J1701−462 in outburst with the *Chandra*'s High-Resolution Camera (HRC-S) in timing mode and they did not find evidence of other sources in the HRC-S field of view (6×90 arcmin^2). *Swift* observations with the X-ray telescope as well as *XMM–Newton* observations of XTE J1701−462 did not show other sources, respectively, within 23.6×23.6 and 30×30 arcmin^2. Finally we checked the *RXTE* Galactic Bulge scans archive and we found that with a spatial accuracy of 15 arcmin no sources have been detected in a 1-deg^2 area from the XTE 1701−462 position. The evidence just discussed indicates that most likely the outburst observed by *RXTE* was due to a single source, XTE J1701−462, switching from Z to atoll.

Another interesting aspect to mention is the mismatch of the frequency of the lower kHz QPOs between the two different phases of the source. It is clear from Tables 1 and 2 and Figs 3 and 4 that Z phase lower kHz QPOs are in the range 500–660 Hz, while in the atoll phase the lower kHz QPOs are in the frequency range 640–860 Hz. Although a similar effect has been observed when one compares other atoll and Z sources (see Méndez 2006 for a compilation), we have now shown this effect in a single source. Studying the energy spectra in different parts of the colour–colour diagram, Lin et al. (2009a) found that in the Z phase the disc is truncated far from the NS surface and its inner radius could be set by the local Eddington limit, while in the atoll phase the disc extends closer to the NS. Different sizes of the inner radius of the accretion disc could explain the different range of kHz QPO frequencies. However, we cannot discard the presence of other lower kHz QPOs in the Z phase at frequencies higher than what we found. From the upper limits for the Z phase reported in Section 3, it is apparent that we are not sensitive enough to detect broad and weak QPOs at high frequencies in that phase.

5 CONCLUSIONS

We studied the properties of the kHz QPOs in the transient source XTE J1701−462, the only source so far that during an outburst underwent a transition from Z to atoll class. We found the following.

(i) Most of the time, when there are kHz QPOs in the Z phase, the power spectrum shows two simultaneous kHz QPOs, whereas in the atoll phase there is only one kHz QPO that we identify as the lower kHz QPO.

(ii) The coherence and fractional rms amplitude of the kHz QPOs are significantly different between the Z and atoll phases. Atoll lower kHz QPOs show quality factors and fractional rms amplitude, respectively, two and three times larger than the Z ones in the same frequency range.

(iii) There is no single Z observation in which the kHz QPOs have a coherence or rms amplitude similar to those seen when XTE J1701−462 was in the atoll phase, even though the total exposure time was about five times longer in the Z than in the atoll phase.

(iv) The difference in QPO properties cannot be due to quantities like NS mass, magnetic field, spin, inclination of the accretion disc, etc. We suggest that this difference is due to a change in the properties of the accretion flow around the NS where the QPOs are produced.

We conclude that, at least in XTE J1701−462, the coherence and rms amplitude of the kHz QPOs are not uniquely driven by the radius in the accretion disc in which QPOs are most probably created.

Our results show that effects other than the geometry of the space–time around the NS have a strong influence on the QPO properties.

ACKNOWLEDGMENTS

This research has made use of data obtained from the High Energy Astrophysics Science Archive Research Center (HEASARC), provided by NASA's Goddard Space Flight Center. This research made use of the SIMBAD data base, operated at CDS, Strasbourg, France and NASA's Astrophysics Data System. MM, DA, TB, PC and MvdK wish to thank ISSI for their hospitality. We thank Didier Barret for interesting discussions that helped us improve the presentation. JH gratefully acknowledges support from NASA grant NNX08AC20G. PC acknowledges funding via a EU Marie Curie Intra-European Fellowship under contract no. 2009-237722. TB acknowledges support from grant PRIN-INAF 2008 and from ASI via contract I/088/06/0, and a visitor grant from NWO.

REFERENCES

Abramowicz M. A., Karas V., Kluzniak W., Lee W. H., Rebusco P., 2003, PASJ, 55, 467
Altamirano D., van der Klis M., Méndez M., Migliari S., Jonker P. G., Tiengo A., Zhang W., 2005, ApJ, 633, 358
Altamirano D., van der Klis M., Méndez M., Wijnands R., Markwardt C., Swank J., 2008, ApJ, 687, 488
Barret D., Kluźniak W., Olive J. F., Paltani S., Skinner G. K., 2005a, MNRAS, 357, 1288
Barret D., Olive J.-F., Miller M. C., 2005b, MNRAS, 361, 855
Barret D., Olive J.-F., Miller M. C., 2005c, Astron. Nachr., 326, 808
Barret D., Olive J.-F., Miller M. C., 2006, MNRAS, 370, 1140
Belloni T., Psaltis D., van der Klis M., 2002, ApJ, 572, 392
Belloni T., Homan J., Motta S., Ratti E., Méndez M., 2007, MNRAS, 379, 247
Berger M. et al., 1996, ApJ, 469, L13
Boutelier M., Barret D., Lin Y., Tö rök, 2010, MNRAS, 401, 1290
Bradt H. V., Rothschild R. E., Swank J. H., 1993, A&AS, 97, 355
Di Salvo T., Méndez M., van der Klis M., Ford E., Robba N. R., 2001, ApJ, 546, 1107
Di Salvo T., Méndez M., van der Klis M., 2003, A&A, 406, 177
Gilfanov M., Revnivtsev M., 2005, Astron. Nachr., 326, 812
Gilfanov M., Revnivtsev M., Molkov S., 2003, A&A, 410, 217
Hasinger G., van der Klis M., 1989, A&A, 225, 79
Homan J., van der Klis M., Jonker P. G., Wijnands R., Kuulkers E., Méndez M., Lewin W. H. G., 2002, ApJ, 568, 878
Homan J., Wijnands R., Altamirano D., Belloni T., 2007a, Astron. Telegram, 1165
Homan J. et al., 2007b, ApJ, 656, 420
Homan J. et al., 2010, submitted (arXiv:1005.3210)
Jahoda K., Markwardt C. B., Radeva Y., Rots A. H., Stark M. J., Swank J. H., Strohmayer T. E., Zhang W., 2006, ApJS, 163, 401
Jonker P. G., Wijnands R., van der Klis M., Psaltis D., Kuulkers E., Lamb F. K., 1998, ApJ, 499, L191
Jonker P. G. et al., 2000, ApJ, 537, 374
Kaaret P., Piraino S., Bloser P. F., Ford E. C., Grindlay J. E., Santangelo A., Smale A. P., Zhang W., 1999, ApJ, 520, L37
Krauss M. I., Juett A. M., Chakrabarty D., Jonker P. G., Markwardt C. B., 2006, Astron. Telegram, 777, 1
Kuulkers E., van der Klis M., Oosterbroek T., Asai K., Dotani T., van Paradijs J., Lewin W. H. G., 1994, A&A, 289, 795
Lee H. C., Miller G. S., 1998, MNRAS, 299, 479
Lin D., Remillard R. A., Homan J., 2009a, ApJ, 696, 1257
Lin D., Altamirano D., Homan J., Remillard R. A., Wijnands R., Belloni T., 2009b, ApJ, 699, 60
Méndez M., 2006, MNRAS, 371, 1925
Méndez M., van der Klis M., 1999, ApJ, 517, L51
Mendez M. et al., 1998, ApJ, 494, L65
Méndez M., van der Klis M., Ford E. C., Wijnands R., van Paradijs J., 1999, ApJ, 511, L49
Méndez M., van der Klis M., Ford E. C., 2001, ApJ, 561, 1016
Miller M. C., Lamb F. K., Cook G. B., 1998a, ApJ, 509, 793
Miller M. C., Lamb F. K., Pslatis D., 1998b, ApJ, 508, 791
Remillard R. A., Lin D., the ASM Team at MIT, NASA/GSFC, 2006, Astron. Telegram, 696, 1
Stella L., Vetri M., 1998, ApJ, 492, L59
Strohmayer T. E., Zhang W., Swank J. H., Smale A., Titarchuk L., Day C., Lee U., 1996, ApJ, 469, L9
van der Klis M., 1997, Astrophys. Space Sci. Library, 218, 121
van der Klis M., 2001, in White N. E., Malaguti G., Palumbo G. G. C., eds, Proc. AIP Conf. Vol. 599, X-ray Astronomy: Stellar Endpoints, AGN, and the Diffuse Stellar Background. Am. Inst. Phys., New York, p. 406
van der Klis M., 2005, Astron. Nachr., 326, 798
van der Klis M., 2006, in Lewin W. H. G., van der Klis M., eds, Compact Stellar X-ray Sources. Cambridge Univ. Press, Cambridge, p. 39
van der Klis M., Swank J. H., Zhang W., Jahoda K., Morgan E. H., Lewin W. H. G., Vaughan B., van Paradijs J., 1996, ApJ, 469, L1
van Straaten S., Ford E. C., van der Klis M., Méndez M., Kaaret P., 2000, ApJ, 540, 1049
van Straaten S., van der Klis M., di Salvo T., Belloni T., 2002, ApJ, 568, 912
van Straaten S., van der Klis M., Méndez M., 2003, ApJ, 596, 1155
Wijnands R. A. D., van der Klis M., van Paradijs J., Lewin W. H. G., Lamb F. K., Vaughan B., Kuulkers E., 1997, ApJ, 479, L141
Wijnands R. A. D. et al., 1998, ApJ, 493, L87

This paper has been typeset from a TEX/LATEX file prepared by the author.